

# Continuous conditional video synthesis by neural processes

Xi Ye

Polytechnique Montréal  
Montréal, Canada

xi.ye@polymtl.ca

Guillaume-Alexandre Bilodeau

Polytechnique Montréal  
Montréal, Canada

guillaume-alexandre.bilodeau@polymtl.ca

## Abstract

*We propose a unified model for multiple conditional video synthesis tasks, including video prediction and video frame interpolation. We show that conditional video synthesis can be formulated as a neural process, which maps input spatio-temporal coordinates to target pixel values given context spatio-temporal coordinates and pixels values. Specifically, we feed an implicit neural representations of coordinates into a Transformer-based non-autoregressive conditional video synthesis model. Our task-specific models outperform previous work for video interpolation on multiple datasets and reach a competitive performance with the state-of-the-art models for video prediction. Importantly, the model is able to interpolate or predict with an arbitrary high frame rate, i.e., continuous synthesis. Our source code is available at <https://github.com/NPVS/NPVS>.*

## 1. Introduction

Video synthesis has been a hot research topic in recent years because of its numerous applications, including video games, computer graphics and robotics. In this paper, we focus on two closely related conditional video synthesis tasks, video frame interpolation (VFI) and video frame prediction (VFP). VFI consists in interpolating intermediate frames between a pair of existing frames, while VFP consists in predicting future frames given some past frames. VFP is harder than VFI because future predictions contain more uncertainties.

Even though VFI and VFP share some similarities, they have been tackled by totally different methods for a long time. For example, most VFI methods capture the motion between input frames by estimating optical flow [1, 2] or local convolution kernels [3, 4]. None of these methods are able to solve the VFP problem. Besides, VFI methods normally require high frame rate videos and rely on neural network models that are trained in a supervised manner to predict the missing intermediate frames given a downsampled low frame rate input video. Meanwhile, most VFP models

depend on Convolutional-LSTMs (ConvLSTMs) to predict the future frames autoregressively [5, 6, 7, 8], and they are incapable of performing video interpolation.

Therefore, in this paper, we address the problem of unifying multiple conditional video synthesis tasks to solve them with a single model. To do so, we propose a novel unsupervised continuous conditional video synthesis method based on neural processes (NPs) [9] and an implicit neural representation (INR) [10, 11]. NPs have been successfully applied for image completion [9, 11], but to the best of our knowledge, this is the first work that successfully achieves conditional video synthesis by neural processes. In addition to VFI and VFP, the flexibility of NPs also enables our model to deal with video past frame extrapolation (VPE) and video random missing frames completion (VRC).

Our first motivation to unify multiple conditional video synthesis tasks with one model is that the two are often required when processing videos. For example, they can contribute to improve object detection and data association in object tracking, as missing frames can be rebuilt with VFI or the video frame rate can be improved, and VFP can be used to predict the context changes surrounding an object in a frame to track it more robustly. Our second motivation is that we believe our unified model could serve as a good self-supervised learning model for various video processing tasks, like activity recognition, because predicting the visual missing parts given contexts is one of the most important self-supervised learning methods [12, 13, 14], and multi-task learning is a good regularization for a better representation learning [15]. One common problem for almost all conditional video synthesis models is that they can only generate video with a fixed frame rate, i.e., discrete synthesis. However, the real world is continuous over the spatio-temporal space. Therefore, our last motivation is to develop a conditional video synthesis model that is able to recover the underlying continuous signal of the real world given a discrete dataset, and thus enable many useful applications, e.g., generating videos with an arbitrary high frame rate, or generating a climate video with irregular time interval [16].

By formulating conditional video synthesis as a neural

process, we build a supervised mapping from any target spatio-temporal coordinate of frames to target pixel values, given observed context coordinates and pixel values. The spatio-temporal coordinates are encoded by an implicit neural representation learning model to achieve continuous generation. More specifically, we firstly extract the features of each video frame by training a convolutional neural network (CNN) autoencoder. Then, a Transformer-based prediction model parameterizes the neural process, which takes the target coordinates as inputs, conditions on context coordinates and context frame features, then outputs the target frame features that are finally fed into the CNN decoder to reconstruct the frame pixels. A Fourier Feature Network (FFN) learns the neural representations of coordinates, which serve as the positional information for the Transformer-based neural process model. We developed a deterministic predictor and a stochastic predictor, where the later one is utilized to deal with tasks with more uncertainty, like VFP and VPE. In summary, our main contributions are:

- We propose the first neural process model for conditional video synthesis (NPVS), which tackles VFP, VFI, VPE and VRC with one model;
- Our work is the first that successfully adapts the implicit neural representation for a temporal continuous VFP;
- The proposed model is able to make temporal continuous video generation, i.e., generating video with an arbitrary high frame rate;
- Our model outperforms the state-of-the-art (SOTA) models for VFI over multiple datasets and achieves a competitive performance with SOTA VFP models.

## 2. Background

**Neural processes (NPs).** Given a set of labeled contexts  $C = (X_C, Y_C) = \{(x_i, y_i)\}_{i \in \mathcal{I}(C)}$  and an unlabeled target set  $T = X_T = \{x_i\}_{i \in \mathcal{I}(T)}$ , Garnelo *et al.* [9] proposed (conditional) neural processes to model the predictive distribution  $p(f(T)|C, T)$ , where  $\mathcal{I}(S)$  denotes the indices of data points in set  $S$ , function  $f : X \rightarrow Y$  defines the mapping from domain  $X$  to  $Y$ . Specifically, the contexts  $C$  are firstly encoded and aggregated into a context embedding of fixed dimension, then  $p(f(T)|C, T)$  is parameterized by a neural network with the inputs of context embedding and  $T$ . NPs are efficient because they preserve merits of both Gaussian processes and deep neural networks. An important property of NPs is that they are permutation invariant in  $C$  and  $T$  [9]. NPs can be extended to a latent variable version that accounts for the uncertainty of  $f(T)$  based on VAE [17]. In order to solve the underfitting problem of NPs, Kim *et al.* [18] proposed to replace the context feature aggregation operation by an attention mechanism. NPs are

required to be with scalability, flexibility and permutation invariance [18], they have been successfully applied for image completion [9, 18, 11]. In this case, the pixel coordinates are considered as  $x_i$  and pixel values are considered as  $y_i$ . Benefiting from the permutation invariance, NPs can predict missing pixel values condition on context pixels in arbitrary patterns.

**Implicit neural representations (INRs).** INRs [10, 11] are techniques which solve the spectral bias problem of neural networks and thus achieve a continuous mapping between the input coordinates and target signal values, e.g., pixel values. There are mainly two different types of INRs. The first one is a Fourier Feature Network (FFN) [10], which uses a Fourier feature mapping for the input of a normal multiple layer perceptron (MLP) to enable the learning of high-frequency signal components effectively. The second one is a SInusoidal REpresentation Network (SIREN) [11]. SIREN depends on periodic activation functions, i.e., sinusoidal activations, to continuously represent the signals with fine details. Both FFN and SIREN are efficient, and some work [19, 20] have proven that they are equivalent to each other. INRs have been adopted for many computer vision tasks, including neural radiance fields for novel view synthesizing [21], image generation [22], unconditional video generation [23] and video interpolation [24].

## 3. Related work

Any video to video synthesis task can be considered as a conditional video synthesis, including video translation between different domains [25], video super-resolution [26, 27], VFI and VFP. We particularly focus on the work related to VFI and VFP. The classical supervised VFI models take optical flow-based [1, 2] or kernel-based methods [3, 4] to learn the motion for the intermediate frames. The drawback is that those models require a high frame rate training dataset, which is relatively expensive to acquire. Some unsupervised VFI models have been proposed in recent years, for example, Reda *et al.* [28] developed a unsupervised VFI model based on cycle consistency. A more recent optical flow-based CNN model, VideoINR [24], successfully utilizes the implicit neural representation for continuous VFI.

VFP models can be categorized into many different types, such as deterministic models [29, 30], stochastic models [31, 5], pixel-direct generation models [30, 32] and transformation-based models [33, 34]. Almost all the VFP models are autoregressive models based on ConvLSTMs or Transformers [35, 36]. Recently, a few promising non-autoregressive VFP models were proposed [37, 38, 39]. By combining ConvLSTMs with a neural ordinary differential equation (ODE) solver, Vid-ODE [16] is the first method that unifies the VFP and VFI into a single model, and it is able to generate temporally continuous video.

Another work, masked conditional video diffusion (MCVD) [39] extends the 3D CNN-based diffusion models for video generation, but it is not an NP model and it is not able to do continuous video synthesis. In contrast, benefiting from the flexibility of NPs, our model is able to perform video random missing frames completion (VRC), which is more flexible than MCVD. Furthermore, our model achieves stochastic prediction based on VAE instead of a diffusion model.

Our model is different from previous work in two aspects. Firstly, none of them are built to be a neural process. We believe that a NP is a better choice because it is permutation invariant in contrast to ConvLSTMs or 3D-CNN that are not. Therefore, they do not have the flexibility of our model to achieve multiple conditional video synthesis tasks with a single model. Vid-ODE [16] is the only one to circumvent this limitation by introducing ODE. However, our NPs-based model outperforms the Vid-ODE for both VFP and VFI, as it will be shown in experiments. Secondly, implicit neural representation (together with NPs) enables our model to predict frames at any given temporal coordinate, even though they are not seen during the training. Most of the previous models can only predict video frames with a fixed frame rate, which is defined by the training dataset. The only exceptions are the aforementioned Vid-ODE [16] and VideoINR [24]. VideoINR can only perform VFI and it does not satisfy the properties of NPs.

## 4. Proposed method

Figure 1 depicts the proposed overall framework. Given some context frames  $V_C \in \mathbb{R}^{L_C \times I_h \times I_w \times I_c}$ , a conditional video generation model is trained to generate some target frames  $V_T \in \mathbb{R}^{L_T \times I_h \times I_w \times I_c}$ , where  $L_C$  and  $L_T$  denote the number of context frames and the number of target frames, respectively.  $I_h, I_w, I_c$  are the image height, width, and the number of color channels. Firstly, the visual feature  $Y_C \in \mathbb{R}^{L_C \times H \times W \times D}$  of context frames are extracted by a frame encoder, then a predictor predicts the target visual feature  $\hat{Y}_T \in \mathbb{R}^{L_T \times H \times W \times D}$  given  $Y_C, X_C$  and  $X_T$ .  $X_C$  and  $X_T$  denotes the context spatio-temporal coordinate encodings and target spatio-temporal coordinate encodings learned by a Fourier Feature Network (Figure 2 (a)).  $X_C \in \mathbb{R}^{L_C \times H \times W \times D}$  and  $X_T \in \mathbb{R}^{L_T \times H \times W \times D}$ ,  $H, W, D$  denote the visual feature height, width and channels. Finally, the target frames are reconstructed by a frame decoder given  $\hat{Y}_T$ .

We divided our model into two parts, a frame autoencoder and a NPs-based predictor that operates over the feature space. The reason for our choice is that directly learning a NPs-based model over the pixel space is expensive. Operating over the feature space allows us to train the model in two stages. We firstly train the frame encoder and frame decoder by ignoring the NPs-based predictor, and then fix

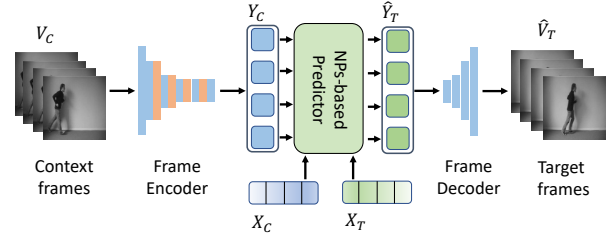


Figure 1. Overall framework.

the parameters of the frame autoencoder to learn the predictor. The detail architectures of the autoencoder, NPs-based Predictors (Figure 2 (b) and Figure 3), and the FFN (Figure 2 (a)) are described in the following.

### 4.1. Autoencoder

We use a custom autoencoder that is adapted from Pix2Pix [40]. Specifically, we integrate four non-local 2d attention layers (orange layers of the frame encoder in Figure 1) from SAGAN [41] into the CNN encoder to improve its performance. There is no modification for the frame decoder of Pix2Pix. The autoencoder is trained with a simple  $L_1$  loss between input frame  $I$  and reconstructed frame  $\hat{I}$ , i.e.,  $\mathcal{L}_1(I, \hat{I}) = |I - \hat{I}|$ . Recall that the predictor is ignored during the learning of the autoencoder, and the autoencoder is fixed during the learning of the predictor.

### 4.2. Fourier feature network for INRs

We select the FFN [10] instead of SIREN [11] because FFN is easier to implement and train. For a visual feature  $y_i \in \mathbb{R}^{H \times W \times D}$  of one frame, where  $i$  is the temporal coordinate, FFN takes the coordinate  $(h, w, i)$  of each feature vector at different spatio-temporal location as input, and outputs a  $D$ -dimensional coordinate encoding for  $(h, w, i)$ . The INR is shown Figure 2 (a).  $x_i \in \mathbb{R}^{H \times W \times D}$  denotes all the spatial-temporal coordinate encodings of a frame feature  $y_i$ .  $X_C$  and  $X_T$  contains all the  $x_i$  of context and target coordinates respectively. Specifically, for an input 3D coordinate vector  $(h, w, i)$ , FFN firstly projects it to a higher dimensional space by a Gaussian random noise matrix, then the projections are fed into a MLP with ReLU activation functions to get the output coordinate encoding. The spatio-temporal coordinates are normalized to the range  $[0, 1]$ . The FFN is jointly learned with the NPs-based predictor.

The implicit neural representations  $X_C$  and  $X_T$  generated by FFN encode the spatio-temporal location information of context features  $Y_C$  and target features  $Y_T$ . They are critical for the learning of our Transformer-based predictor (section 4.3) because a Transformer is permutation invariant. After training, INRs are able to generalize to unseen input coordinates, which means we can get the coordinate encoding  $x_i$  at any real-number temporal coordinate  $i$ . Because the model predicts different  $y_i$  given contexts

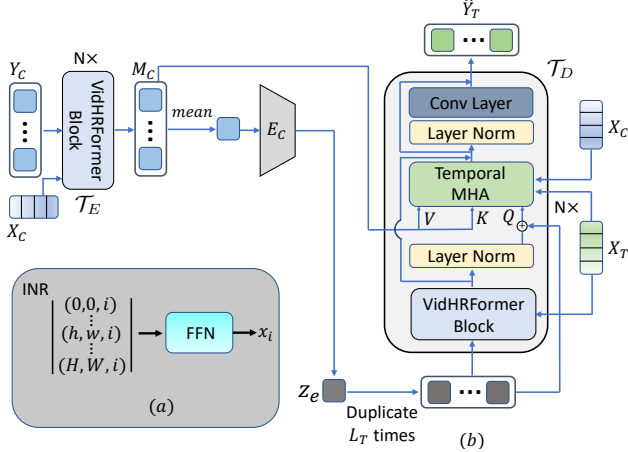


Figure 2. (a) INR (b) Deterministic Predictor (NPVS-D).

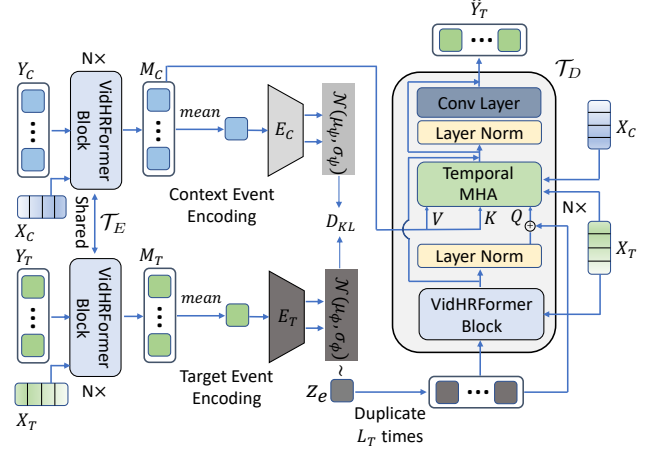


Figure 3. Stochastic Predictor (NPVS-S).

and different target  $x_i$  (section 4.3), we can achieve a continuous generation. For VFP task, if we need to predict target frames beyond the maximum temporal coordinates used during training, we can perform a "block-wise" autoregressive prediction. Specifically, take the predicted future (target) frames as the past (context) frames for the next block of future (target) frames.

### 4.3. NPs-based Predictors

We proposed a deterministic (NPVS-D) and a stochastic predictor (NPVS-S). The deterministic model has a simpler architecture and is easier to train. But NPVS-D cannot take into account the randomness and only predicts the average of all possible outcomes [31]. Therefore, a stochastic model is also desirable. For example, a ball with random motion can move toward any direction, even though we will observe only one outcome. The stochastic predictor can generate different random predictions for the same contexts.

Both predictors are implemented as attentive neural processes [18] based on a video representation learning Transformer, VidHRFormer [38]. This is motivated by the fact that attentive neural process preserves the permutation invariance and solves the underfitting problem of a vanilla NP, and VidHRFormer satisfies all the requirements of attentive neural processes. Besides, VidHRFormer has been successfully used for efficient VFP [38], and Transformers exhibit good scaling properties in computer vision [42, 43].

**Deterministic Predictor (NPVS-D).** Given contexts  $(X_C, Y_C)$  and  $X_T$ , a NP models the conditional distribution  $p(Y_T|X_C, Y_C, X_T)$ . We model  $p$  as a Laplacian distribution with a constant scale parameter. Then, maximizing the log-likelihood is equivalent to minimizing a  $L_1$  loss, that is  $|Y_T - \hat{Y}_T|$ . However, in practice, we find that learning with the  $L_1$  loss over the latent feature space alone is not enough to generate predictions with good visual quality as we will discuss later in the ablation study. Therefore, we feed  $\hat{Y}_T$  to

the fixed frame decoder to reconstruct a frame  $\hat{V}_T$  and minimize another pixel reconstruction  $L_1$  loss at the same time. Then, the loss function of the deterministic NP predictor is

$$\mathcal{L}_{det} = |V_T - \hat{V}_T| + \gamma|Y_T - \hat{Y}_T|, \quad (1)$$

where  $\gamma$  is a hyperparameter.

In detail, the architecture of our deterministic predictor can be formalized by these operations,

$$M_C = \mathcal{T}_E(X_C, Y_C) \quad (2)$$

$$z_e = E_C(\text{mean}(M_C)) \quad (3)$$

$$\hat{Y}_T = \mathcal{T}_D(X_T, X_C, M_C, z_e), \quad (4)$$

where  $\mathcal{T}_E : X_C \times Y_C \rightarrow M_C \in \mathbb{R}^{L_C \times H \times W \times D}$  denotes the context Transformer encoder, which is composed by multiple VidHRFormer blocks [38] (see supplementary material for the detail architecture). The spatio-temporal separated attention mechanism of VidHRFormer block ensures the permutation invariance along the temporal dimension.  $X_C$  is fused into  $\mathcal{T}_E$  as the positional encodings. We hypothesize that all target visual features are generated by a latent representation  $z_e \in \mathbb{R}^{H \times W \times D}$ , which is named as "event variable". In order to generate  $z_e$ ,  $M_C$  is firstly averaged along the temporal dimension, then passed through an event encoder  $E_C : \mathbb{R}^{H \times W \times D} \rightarrow \mathbb{R}^{H \times W \times D}$ , where  $E_C$  is a small CNN (see supplementary material for the detail architecture). We use *mean* operation because it is an efficient aggregation method and it is permutation invariant.

Finally,  $\hat{Y}_T$  is generated by conditioning on  $(X_T, X_C, M_C, z_e)$  through another Transformer  $\mathcal{T}_D$ . The architecture of the  $\mathcal{T}_D$  block is same as the Transformer decoder block of VPTR [38]. Note that we duplicate the event variable  $L_T$  times and feed it into  $\mathcal{T}_D$  as the initial query for each target frame feature.  $X_T$  is injected into  $\mathcal{T}_D$  as positional encodings. In this way, we can generate  $\hat{Y}_T$  with arbitrary frame rate, i.e., continuously prediction, as

long as we input the desired  $X_T$ , which is produced by the trained FFN for free. On the contrary, VPTR [38] could only predict future frames with a fixed frame rate due the limitation of a fixed number of learned frame queries.

**Stochastic Predictor (NPVS-S).** NPVS-D can be extended to be stochastic, see Figure 3. The difference is that we assume  $z_e$  to be randomly sampled from a learned event space, instead of simply be deterministically derived from the contexts, and thus  $z_e$  explains the uncertainty during the prediction of  $Y_T$ . Theoretically, we can describe the generative process of  $Y_T$  as:

$$p(Y_T|X_C, Y_C, X_T) = \int p(Y_T|X_T, X_C, Y_C, z_e)q(z_e|X_C, Y_C)dz_e, \quad (5)$$

where  $q(z_e|X_C, Y_C)$  defines a conditional prior distribution for  $z_e$ . By adapting a VAE [17], we can learn the stochastic NP by maximizing the evidence lower bound (ELBO):

$$ELBO = \mathbb{E}_{q_\phi(z_e|X_T, Y_T)}[\log p(Y_T|X_T, X_C, Y_C, z_e)] - \beta D_{KL}(q_\phi(z_e|X_T, Y_T)||q_\psi(z_e|X_C, Y_C)), \quad (6)$$

where  $\beta$  is a hyperparameter. Specifically, the first term of the right-hand side of Eq. 6 can be parameterized the same way as the deterministic predictor, i.e., Eq. 1, which forces the predictor to reconstruct  $Y_T$ . The KL divergence is a regularization term that prevents the  $z_e$  sampled from targets to deviate too far from the  $z_e$  sampled from the context, with the assumption that both context frames and target frames are generated from the same latent event space. During training,  $z_e$  is sampled from a factorized Gaussian distribution  $\mathcal{N}(\mu_\phi, \sigma_\phi)$  via the reparameterization trick, and

$$\mu_\phi, \sigma_\phi = E_T(\text{mean}(M_T)) \quad (7)$$

$$= E_T(\text{mean}(\mathcal{T}_E(X_T, Y_T))), \quad (8)$$

where  $E_T$  is the target event encoder. Eq. 8 formalizes the detail architecture of the target event encoding path in Figure 3. During test, the ground truth  $Y_T$  is not accessible, then  $z_e$  is sampled from the learned context prior event space  $\mathcal{N}(\mu_\psi, \sigma_\psi)$ , which is generated by the context event encoding path of Figure 3, i.e.,

$$\mu_\psi, \sigma_\psi = E_C(\text{mean}(M_C)) \quad (9)$$

$$= E_C(\text{mean}(\mathcal{T}_E(X_C, Y_C))). \quad (10)$$

## 5. Experiments

We evaluate the proposed predictors on two realistic video datasets, KTH [45], BAIR [46], and a synthetic video dataset, Stochastic Moving MNIST (SM-MNIST) [5]. All datasets are resized to the resolution of  $64 \times 64$ . Please see the supplementary material for the implementation details.

Following the experimental configuration of previous works, we present the quantitative results of Peak Signal-to-Noise Ratio (PSNR), Fréchet Video Distance (FVD)[47], Learned Perceptual Image Patch Similarity (LPIPS)[48] and Structural Similarity Index Measure (SSIM). The LPIPS is reported in  $10^{-3}$  scale. The average metrics are reported for deterministic models. Same as in previous work, for stochastic models, 100 different predictions are sampled for each test example, then the best SSIM, LPIPS, PSNR and the average FVD of the generated samples are reported.

For a fair comparison with previous task-specific models, we firstly train different models for VFP and VFI respectively, i.e., we train task-specific models following the same training procedures that they used. After that we will present results with a unified model that is not task-specific.

### 5.1. Task-specific models

**VFI.** For the VFI task, given  $p$  past frames and  $f$  future frames as the context, the model is trained to generate  $k$  intermediate frames, i.e., target frames. For VFI, the context span across the past and future, which limits the stochasticity of the event. Therefore, the deterministic model is applied to all datasets, even for the datasets with more randomness, like BAIR and SM-MNIST.

The VFI results are summarized in Table 1. For the KTH dataset, our task-specific deterministic *NPVS-D* ( $15 \rightarrow 10$ ) model outperforms the SOTA MCVD ( $15 \rightarrow 10$ ) in terms of SSIM. It also outperforms Vid-ODE in terms of all metrics by a large margin. Note that a smaller  $p + f$  and a larger  $k$  means a harder VFI task. Therefore we can safely draw the conclusion that our model is better than SVG-LP and SDVI full too, because ( $15 \rightarrow 10$ ) is harder than ( $18 \rightarrow 7$ ). Our *NPVS-D* ( $10 \rightarrow 5$ ) also outperforms MCVD ( $10 \rightarrow 5$ ) model in terms of both SSIM and PSNR. The *NPVS-D* ( $10 \rightarrow 5$ ) outperforms *NPVS-D* ( $15 \rightarrow 10$ ). We believe that it is because 10 context frames are enough to provide good context information for KTH datasets, and interpolating 5 frames is much easier than interpolating 10 frames.

For SM-MNIST dataset, our deterministic *NPVS-D* ( $10 \rightarrow 10$ ) outperforms all the previous methods in terms of both PSNR and SSIM, even for the easier ( $18 \rightarrow 7$ ) and ( $10 \rightarrow 5$ ) tasks. It means that given the same number of context frames, our model is able to interpolate more intermediate frames with better quality. Furthermore, MCVD samples multiple possible predictions for each test example and reports the best metrics. In contrast, our deterministic model only makes one inference. The *NPVS-D* ( $10 \rightarrow 5$ ) outperforms *NPVS-D* ( $10 \rightarrow 10$ ) by a large margin as expected. In short, the results demonstrate that a deterministic model is capable of achieving good VFI for KTH and SM-MNIST datasets, even though the latter one has more uncertainty.

For BAIR dataset, our deterministic *NPVS-D* ( $18 \rightarrow 7$ ) outperforms SVG-LP and SDVI full by a large margin.

Models	KTH				SM-MNIST				BAIR			
	$(p+f \rightarrow k)$	PSNR $\uparrow$	SSIM $\uparrow$	LPIPS $\downarrow$	$(p+f \rightarrow k)$	PSNR $\uparrow$	SSIM $\uparrow$	LPIPS $\downarrow$	$(p+f \rightarrow k)$	PSNR $\uparrow$	SSIM $\uparrow$	LPIPS $\downarrow$
SVG-LP [5]	$(18 \rightarrow 7)$	28.13	0.883	-	$(18 \rightarrow 7)$	13.54	0.741	-	$(18 \rightarrow 7)$	18.65	0.846	-
SDVI full [44]	$(18 \rightarrow 7)$	29.19	0.901	-	$(18 \rightarrow 7)$	16.03	0.842	-	$(18 \rightarrow 7)$	21.43	0.880	-
Vid-ODE [16]	-	31.77	0.911	48	-	-	-	-	-	-	-	-
MCVD [39]	$(15 \rightarrow 10)$	34.67	0.943	-	$(10 \rightarrow 10)$	20.94	0.854	-	$(4 \rightarrow 5)$	<b>25.16</b>	<b>0.932</b>	-
MCVD [39]	$(10 \rightarrow 5)$	<b>35.61</b>	<b>0.963</b>	-	$(10 \rightarrow 5)$	27.69	0.940	-	-	-	-	-
<i>NPVS-D</i> (ours)	$(15 \rightarrow 10)^\dagger$	33.25	0.959	<b>23.76</b>	$(10 \rightarrow 10)$	<b>28.77</b>	<b>0.975</b>	<b>17.41</b>	$(18 \rightarrow 7)$	22.29	0.903	24.87
	$(10 \rightarrow 5)$	<b>36.89</b>	<b>0.978</b>	<b>6.68</b>	$(10 \rightarrow 5)$	<b>34.19</b>	<b>0.994</b>	<b>4.52</b>	$(4 \rightarrow 5)$	23.22	0.914	22.48
<i>NPVS-S</i> (ours)	-	-	-	-	-	-	-	-	$(18 \rightarrow 7)$	22.97	0.909	<b>21.78</b>
	-	-	-	-	-	-	-	-	$(4 \rightarrow 5)$	<b>25.28</b>	<b>0.933</b>	<b>14.66</b>

Table 1. VFI results.  $p$  and  $f$  denotes the number of past frames and number of future frames respectively,  $k$  denotes the number of intermediate frames to interpolate. **Smaller  $p+f$  and larger  $k$  means a harder VFI task.**  $\dagger$ :  $p = 8, f = 7$ ; for our other models,  $p$  equals to  $f$ . **Boldface**: best results. **Blue**: second best results.

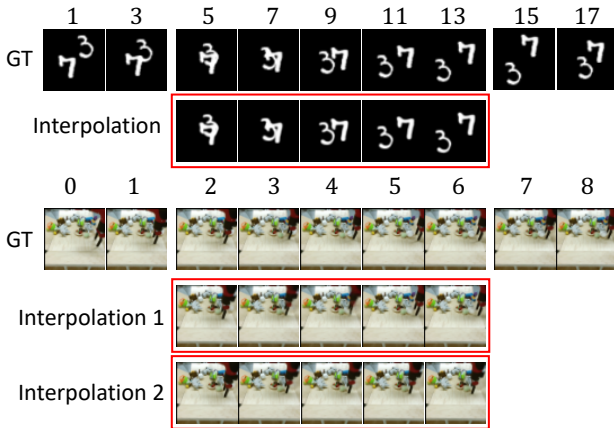


Figure 4. VFI examples on SM-MNIST and BAIR. For stochastic VFI of BAIR, different robot arm shapes and movements are observed between two interpolations.

However, we observe that there is a performance gap between *NPVS-D* ( $4 \rightarrow 5$ ) and MCVD ( $4 \rightarrow 5$ ). The reason is that the robot arm position in each frame of BAIR is independent from other frames, i.e., fully random across the temporal dimension, thus it is difficult to learn the motion of intermediate frames given context frames, unlike KTH, where the natural human motion in missing frames are mostly constrained by the past and future movements. It is the same case for SM-MNIST, where the randomness only occurs when the characters bounce off the boundaries. Most of the times, the character trajectories of intermediate frames can be predicted based on the past and future frames. Therefore, we trained a stochastic *NPVS-S* ( $4 \rightarrow 5$ ) model for VFI on BAIR, where 100 random interpolations are generated for each example and we report the best metric, same as MCVD ( $4 \rightarrow 5$ ). The *NPVS-S* ( $4 \rightarrow 5$ ) improves the performance in terms of all metrics as we expected and it also outperforms MCVD. Compared with *NPVS-D* ( $18 \rightarrow 7$ ), a similar performance boost is observed for *NPVS-S* ( $18 \rightarrow 7$ ).

Other than achieving a new SOTA for VFI, our models can interpolate with an arbitrary high frame rate, while all other models, except Vid-ODE, are not equipped with this continuous interpolation ability. Visual examples of our deterministic VFI on SM-MNIST and stochastic VFI on BAIR are shown in Figure. 4. Please see the supplementary material for more qualitative results.

**VFP.** A deterministic *NPVS-D* model and a stochastic *NPVS-S* model are trained for VFP on each dataset. The VFP experimental results are summarized in Table 2. For the KTH dataset, the models are trained to predict 10 future frames given 10 past frames. During test, the performance is evaluated on predicting 20 future frames conditioned on 10 past frames, which is achieved by a block-wise autoregressive inference. Our *NPVS-D* achieves the best LPIPS and the second best SSIM on KTH. However, we find that the *NPVS-S* model is worse than its deterministic counterpart. We observed that training of the *NPVS-S* model can be unstable and the reasons are discussed in the ablation study.

For the SM-MNIST dataset, the models predict 10 future frames given 5 past frames for both training and test. Our *NPVS-D* achieves the best SSIM, but we observe a large performance gap between our model and the SOTA in terms of FVD and LPIPS. By examining some prediction examples, we find that the visual quality of the last few frames quickly degrades and they make the whole video clip look unrealistic, which is exactly what FVD and LPIPS focus on. An unstable training of the *NPVS-S* on SM-MNIST is also observed, similar to the stochastic model on KTH. Thus, the performance of *NPVS-S* is worse than *NPVS-D*.

For the BAIR dataset, the models are trained to predict 10 future frames given 2 past frames, but 28 future frames are predicted by block-wise autoregressive inference during test. Our deterministic model reaches a comparable performance with previous work. Similar to the VFI task, *NPVS-S* on BAIR dataset outperforms *NPVS-D* and reaches the second best performance in terms of all three metrics. Different from KTH and SM-MNIST, the training of our stochas-

Models	KTH			SM-MNIST			BAIR			
	$10 \rightarrow 20$			$5 \rightarrow 10$			$2 \rightarrow 28$			
	PSNR $\uparrow$	SSIM $\uparrow$	LPIPS $\downarrow$	FVD $\downarrow$	SSIM $\uparrow$	LPIPS $\downarrow$	PSNR $\uparrow$	SSIM $\uparrow$	LPIPS $\downarrow$	
PredRNN++ [49]	28.47	0.865	228.9	SVG-LP [5]	90.81	0.688	<b>153.0</b>	17.72	0.815	60.3
STMNet [50]	<b>29.85</b>	0.893	118.1	Hier-VRNN [53]	57.17	0.760	<b>103.0</b>	-	0.829	<b>55.0</b>
E3D-LSTM [51]	<b>29.31</b>	0.879	-	STMNet [50]	-	-	-	<b>21.02</b>	<b>0.844</b>	93.6
Conv-TT-LSTM [52]	28.36	<b>0.907</b>	133.4	VPTR-NAR [38] $\dagger$	-	-	-	17.77	0.813	70.0
Vid-ODE [16]	28.19	0.878	80	MCVD-concat [39]	<b>25.63</b>	0.786	-	17.70	0.797	-
VPTR-NAR [38]	26.96	0.879	86.1	MCVD-spatin [39]	<b>23.86</b>	0.780	-	17.70	0.789	-
<i>NPVS-D</i> (ours)	27.51	<b>0.906</b>	<b>65.1</b>	<i>NPVS-D</i> (ours)	89.64	<b>0.868</b>	221.2	17.47	0.817	65.6
<i>NPVS-S</i> (ours)	26.69	0.890	<b>73.5</b>	<i>NPVS-S</i> (ours)	95.69	<b>0.817</b>	188.7	<b>18.15</b>	<b>0.842</b>	<b>57.43</b>

Table 2. VFP results on KTH, SM-MNIST and BAIR.  $\dagger$ : We used the authors’ implementation to obtain these results. Authors only provided a prediction for 10 frames. **Boldface**: best results. **Blue**: second best results.

tic model on BAIR is more stable, which may relate to the value of the hyperparameter  $\beta$ . Please see the supplementary material for qualitative results of VFP.

## 5.2. A unified model for VFI, VFP, VPE and VRC

We trained a deterministic predictor on the KTH dataset to demonstrate that our NPs-based conditional video synthesis model is flexible enough to perform VFI, VFP, video past frame extrapolation (VPE), and video random missing frames completion (VRC) with one single learned model. More importantly, all the aforementioned tasks can be solved with an arbitrary high frame rate, i.e., a continuous synthesis. In order to learn one model for all tasks, we trained the predictor with random contexts, i.e., given a video clip with  $L$  frames, we randomly sample  $L_C$  frames as contexts and the remaining  $L_T = L - L_C$  frames are target frames, together with their corresponding coordinates.  $L = 20$ , and the value of  $L_C$  varies in the range of [4, 16].

In Figure 5, we present examples of one model for all four different conditional video synthesis tasks. The first row is the ground-truth (GT) frames. The frames inside a red box are target frames generated by the model given the other context frames. We can observe that the target frames visual quality of VRC and VFI is better than the VPE and VFP, because VPE and VFP only observe the future or past frames, thus there are more uncertainties and it is harder to predict target frames. On the contrary, the context frames of VRC and VFI are scattered across the temporal dimension, which provides more accurate context motion information about the ground-truth event. Because the model tends to minimize the loss quickly by solving the easier tasks, the model trained with random contexts needs more epochs to reach a comparable performance on VFP and VPE tasks compared to a model trained specifically for that task.

Besides, we investigated the quantitative change of target frames visual quality w.r.t. the varying number of context frames for VFP and VFI (Figure 6). The results demonstrate that all three metrics of quality monotonically increase as more context frames are fed into the model. That is, the

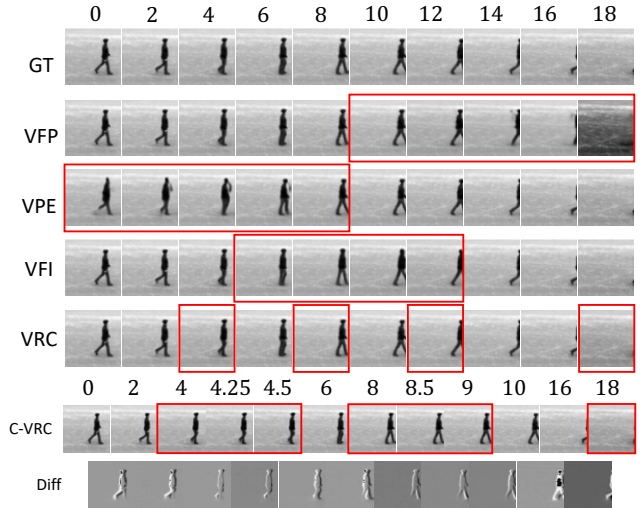


Figure 5. One model for all tasks. Frames inside the red boxes are target frames generated by the model. C-VRC denotes continuous VRC. Diff are the difference images between neighboring frames of C-VRC to show that they are all different and that the temporal coordinates are taken into account.

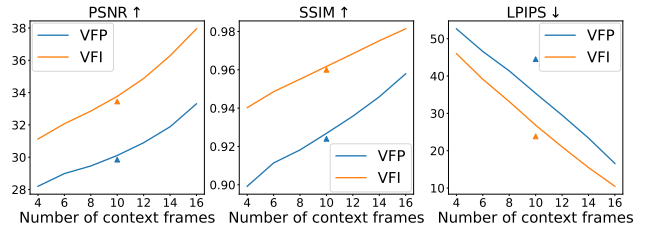


Figure 6. Metric curves of VFP and VFI on KTH for an increasing number of context frames.  $\blacktriangle$  and  $\blacktriangleleft$  denote results of task-specific *NPVS-D* ( $10 \rightarrow 10$ ) for VFI and VFP respectively.

model generates more accurate target frames given more context frames, which is in alignment with the property of NP models [9]. Figure 6 also shows the performance gap between VFP and VFI, which indicates that VFI is an easier task. Results of the deterministic task-specific *NPVS-*

	Models						VFI			VFP		
							$5+5 \rightarrow 10$			$10 \rightarrow 10$		
	$\mathcal{T}_D$ -B	$\mathcal{T}_D$ -L	$\mathcal{T}_E$	$FL_1$	$PL_1$	$D_{KL}$	PSNR $\uparrow$	SSIM $\uparrow$	LPIPS $\downarrow$	PSNR $\uparrow$	SSIM $\uparrow$	LPIPS $\downarrow$
1	✓			✓			31.34	0.953	37.03	28.83	0.920	71.04
2	✓			✓	✓		33.17	0.958	31.11	29.60	0.920	62.96
3		✓		✓	✓		<b>33.20</b>	<b>0.959</b>	29.64	<b>29.85</b>	<b>0.922</b>	<b>57.49</b>
4		✓	✓	✓	✓		<b>33.77</b>	<b>0.962</b>	<b>26.83</b>	<b>30.11</b>	<b>0.927</b>	<b>53.89</b>
5		✓	✓	✓	✓	✓	32.16	0.952	<b>20.90</b>	28.79	0.908	58.70

Table 3. Ablation Study on KTH dataset, trained with random contexts.  $FL_1$  denotes feature space  $L_1$  loss.  $PL_1$  denotes pixel space  $L_1$  loss. Model 5 is the stochastic counterpart of model 4. **Boldface**: best results. *Blue*: second best results.

$D$  ( $10 \rightarrow 10$ ) for VFI and VFP models are plotted in Figure 6. The unified model slightly outperforms the task-specific models in terms of almost all metrics for both VFI and VFP, except for the LPIPS of VFI. Furthermore, we observe from the generated videos that the continuous prediction by the unified model has a better temporal consistency than task-specific models. Therefore, the results validate our second motivation that multi-task learning is beneficial.

Finally, a continuous video random missing frames completion (C-VRC) (Figure 5, bottom) experiment was conducted to show the continuous generation ability of our model. We observe that it is capable of generating frames at unseen temporal coordinates, such as 4.25, 4.5, 8.5. Therefore, theoretically we can do conditional video synthesis at an arbitrary high frame rate.

### 5.3. Ablation study

The base model (model 1) for this study is a deterministic model with a 6-layers of  $\mathcal{T}_D$  ( $\mathcal{T}_D$ -B), which is trained only by a  $L_1$  loss over feature space. We gradually modify the architecture and loss function to investigate the influence of the various components. All models are trained with random contexts and thus we evaluate the performance of both VFI and VFP. For VFI, we take 5 past frames and 5 future frames as input to predict 10 intermediate frames. For VFP, we take 10 past frames as input to predict 10 future frames.

**Pixel  $L_1$  loss.** By introducing the pixel  $L_1$  loss, we observe performance improvement in terms of almost all metrics. Particularly for LPIPS, model 2 outperforms model 1 by a large margin. It proves that pixel  $L_1$  loss is beneficial to the target frames visual quality.

**Size of  $\mathcal{T}_D$ .** In order to investigate the influence of the size of  $\mathcal{T}_D$ , we increase the layer number of  $\mathcal{T}_D$  from 6 to 8 ( $\mathcal{T}_D$ -L). Comparing the results of model 3 with model 2, we observe a performance boost for all metrics of VFI and VFP, which indicates that a larger  $\mathcal{T}_D$  is useful. Besides, the LPIPS gets a larger improvement than SSIM and PSNR.

**Context Transformer encoder  $\mathcal{T}_E$ .** For Model 1-3, there is no explicit temporal relationship learning among context frame features. Because a good aggregation of the context information is critical to improve the performance of NPs, we now include the context Transformer  $\mathcal{T}_E$ , which

models the temporal relationship of  $Y_C$  and generates  $M_C$  for the  $\mathcal{T}_D$  and  $z_e$ . Comparing model 4 with previous models, we observe further improvement over all metrics for both VFP and VFI, especially for the LPIPS metric.

**Stochastic vs Deterministic.** Finally, we convert the model 4 to be stochastic (model 5) by introducing the VAE architecture. During test, we sample 100 different times for each context and report the best average metrics. Model 5 has a worse performance than model 4, except for the LPIPS of VFI, due to the unstable training after introducing the VAE, which leads to a worse convergence. This particularly affects VFP as that there is less uncertainty for VFI, and VFI is easier than VFP. Therefore, a bad optimization of the model would have more effect on a harder task, like VFP.

We also observe a low variety among different random samples of VFP, i.e., mode collapsing. We suspect that there are two reasons: 1) it is particularly hard to find a good value for the hyperparameter  $\beta$ , which leads to the mode collapsing and the unstable training. Some other VAE-based stochastic VFP models encounter a similar problem. For example, SV2P [31] proposed a three stages training strategy to achieve stable optimization of VAE. 2) we only take one latent variable, i.e., a time-invariant latent variable, to account for the stochasticity of whole video sequence, which is limited by the framework of the stochastic NPs. Integrating a time-variant latent variable or hierarchical latent variable could be a potential solution.

## 6. Conclusion

We propose a novel continuous conditional video synthesis model based on neural processes and implicit neural representation. By training with random contexts, we can solve multiple conditional video synthesis tasks with only one model, including video future frame prediction, video frame interpolation, video past frame extrapolation and video random missing frame completion. Importantly, all the tasks can be tackled with an arbitrary high frame rate. Results show that our model achieves the SOTA for video frame interpolation over multiple datasets and reaches a comparable performance with the SOTA models for video future frame prediction.



## References

- [1] Huaizu Jiang, Deqing Sun, Varun Jampani, Ming-Hsuan Yang, Erik Learned-Miller, and Jan Kautz. Super SloMo: High Quality Estimation of Multiple Intermediate Frames for Video Interpolation. In *CVPR*, 2018.
- [2] S. Niklaus and F. Liu. Softmax Splatting for Video Frame Interpolation. In *CVPR*, pages 5436–5445, 2020.
- [3] Simon Niklaus, Long Mai, and Feng Liu. Video Frame Interpolation via Adaptive Convolution. pages 670–679, 2017.
- [4] Simon Niklaus, Long Mai, and Oliver Wang. Revisiting Adaptive Convolutions for Video Frame Interpolation. pages 1099–1109, 2021.
- [5] Emily Denton and Rob Fergus. Stochastic Video Generation with a Learned Prior. In *ICML*, 2018.
- [6] Y. Kwon and M. Park. Predicting Future Frames Using Retrospective Cycle GAN. In *CVPR*, 2019.
- [7] Zheng Chang, Xinfeng Zhang, Shanshe Wang, Siwei Ma, Yan Ye, Xinguang Xiang, and Wen Gao. MAU: A Motion-Aware Unit for Video Prediction and Beyond. In *NeurIPS*, May 2021.
- [8] Sangmin Lee, Hak Gu Kim, Dae Hwi Choi, Hyung-II Kim, and Yong Man Ro. Video Prediction Recalling Long-Term Motion Context via Memory Alignment Learning. In *CVPR*, 2021.
- [9] Marta Garnelo, Dan Rosenbaum, Christopher Maddison, Tiago Ramalho, David Saxton, Murray Shanahan, Yee Whye Teh, Danilo Rezende, and S. M. Ali Eslami. Conditional Neural Processes. In *ICML*, 2018.
- [10] Matthew Tancik, Pratul Srinivasan, Ben Mildenhall, Sara Fridovich-Keil, Nithin Raghavan, Utkarsh Singhal, Ravi Ramamoorthi, Jonathan Barron, and Ren Ng. Fourier Features Let Networks Learn High Frequency Functions in Low Dimensional Domains. In *NeurIPS*, 2020.
- [11] Vincent Sitzmann, Julien Martel, Alexander Bergman, David Lindell, and Gordon Wetzstein. Implicit Neural Representations with Periodic Activation Functions. In *NeurIPS*, 2020.
- [12] Yann LeCun and Ishan Misra. Self-supervised learning: The dark matter of intelligence, 2021.
- [13] Aaron van den Oord, Yazhe Li, and Oriol Vinyals. Representation Learning with Contrastive Predictive Coding. In *arXiv:1807.03748 [cs, stat]*, January 2019. arXiv: 1807.03748.
- [14] Carl Doersch, Abhinav Gupta, and Alexei A. Efros. Unsupervised Visual Representation Learning by Context Prediction. pages 1422–1430, 2015.
- [15] Ian Goodfellow, Yoshua Bengio, and Aaron Courville. *Deep Learning*. MIT Press, November 2016.
- [16] Sunghyun Park, Kangyeol Kim, Junsoo Lee, Jaegul Choo, Joonseok Lee, Sookyung Kim, and Edward Choi. Vid-ODE: Continuous-Time Video Generation with Neural Ordinary Differential Equation. In *AAAI*, May 2021.
- [17] Diederik P. Kingma and Max Welling. Auto-Encoding Variational Bayes. In *ICLR*, 2014.
- [18] Hyunjik Kim, Andriy Mnih, Jonathan Schwarz, Marta Garnelo, Ali Eslami, Dan Rosenbaum, Oriol Vinyals, and Yee Whye Teh. Attentive Neural Processes. In *ICLR*, 2019.
- [19] Nuri Benbarka, Timon Höfer, Hamd ul-Moqheet Riaz, and Andreas Zell. Seeing Implicit Neural Representations As Fourier Series. In *WACV*, 2022.
- [20] Gizem Yüce, Guillermo Ortiz-Jiménez, Beril Besbinar, and Pascal Frossard. A Structured Dictionary Perspective on Implicit Neural Representations. In *CVPR*, 2022.
- [21] Ben Mildenhall, Pratul P. Srinivasan, Matthew Tancik, Jonathan T. Barron, Ravi Ramamoorthi, and Ren Ng. NeRF: Representing Scenes as Neural Radiance Fields for View Synthesis. In Andrea Vedaldi, Horst Bischof, Thomas Brox, and Jan-Michael Frahm, editors, *ECCV*, 2020.
- [22] Ivan Skorokhodov, Savva Ignatyev, and Mohamed Elhoseiny. Adversarial Generation of Continuous Images. In *CVPR*, 2021.
- [23] Ivan Skorokhodov, Sergey Tulyakov, and Mohamed Elhoseiny. StyleGAN-V: A Continuous Video Generator With the Price, Image Quality and Perks of StyleGAN2. In *CVPR*, 2022.
- [24] Zeyuan Chen, Yinbo Chen, Jingwen Liu, Xingqian Xu, Vidit Goel, Zhangyang Wang, Humphrey Shi, and Xiaolong Wang. VideoINR: Learning Video Implicit Neural Representation for Continuous Space-Time Super-Resolution. In *CVPR*, 2022.
- [25] Ting-Chun Wang, Ming-Yu Liu, Jun-Yan Zhu, Guilin Liu, Andrew Tao, Jan Kautz, and Bryan Catanzaro. Video-to-Video Synthesis. In *Advances in Neural Information Processing Systems*, volume 31, 2018.
- [26] Muhammad Haris, Gregory Shakhnarovich, and Norimichi Ukita. Recurrent Back-Projection Network for Video Super-Resolution. In *CVPR*, 2019.
- [27] E. Pérez-Pellitero, M. S. M. Sajjadi, M. Hirsch, and B. Schölkopf. Photorealistic video super resolution. In *Workshop and challenge on perceptual image restoration and manipulation (PIRM) at the 15th european conference on computer vision (ECCV)*, 2018.
- [28] Fitsum A. Reda, Deqing Sun, Aysegul Dundar, Mohammad Shoeybi, Guilin Liu, Kevin J. Shih, Andrew Tao, Jan Kautz, and Bryan Catanzaro. Unsupervised Video Interpolation Using Cycle Consistency. pages 892–900, 2019.
- [29] Y. Wu, R. Gao, J. Park, and Q. Chen. Future Video Synthesis With Object Motion Prediction. In *CVPR*, 2020.
- [30] Xinyuan Chen, Chang Xu, Xiaokang Yang, and Dacheng Tao. Long-term video prediction via criticization and retrospection. *IEEE Transactions on Image Processing*, 29:7090–7103, 2020.
- [31] Mohammad Babaeizadeh, Chelsea Finn, Dumitru Erhan, Roy Campbell, and Sergey Levine. Stochastic variational video prediction. In *ICLR*, 2018.
- [32] Jean-Yves Franceschi, Edouard Delasalles, Mickael Chen, Sylvain Lamprier, and Patrick Gallinari. Stochastic Latent Residual Video Prediction. In *ICLR*, 2020.

- [33] Xionghao Chen, Wenmin Wang, Jinzhuo Wang, and Weimian Li. Learning object-centric transformation for video prediction. In *MM 2017 - Proceedings of the 2017 ACM Multimedia Conference*, pages 1503–1512, 2017.
- [34] B. Jin, Y. Hu, Y. Zeng, Q. Tang, S. Liu, and J. Ye. VarNet: Exploring Variations for Unsupervised Video Prediction. In *IROS*, 2018.
- [35] Wilson Yan, Yunzhi Zhang, Pieter Abbeel, and Aravind Srinivas. VideoGPT: Video Generation using VQ-VAE and Transformers. In *arXiv:2104.10157 [cs]*, September 2021. arXiv: 2104.10157.
- [36] Chenfei Wu, Jian Liang, Lei Ji, Fan Yang, Yuejian Fang, Daxin Jiang, and Nan Duan. N<sup>2</sup>UWA: Visual Synthesis Pre-training for Neural Video World creation. *arXiv:2111.12417 [cs]*, November 2021.
- [37] Zhouyong Liu, Shun Luo, Wubin Li, Jingben Lu, Yufan Wu, Chunguo Li, and Luxi Yang. ConvTransformer: A Convolutional Transformer Network for Video Frame Synthesis. In *arXiv:2011.10185 [cs]*, November 2020.
- [38] Xi Ye and Guillaume-Alexandre Bilodeau. VPTR: Efficient Transformers for Video Prediction. In *26th International Conference on Pattern Recognition (ICPR)*, 2022.
- [39] Vikram Voleti, Alexia Jolicoeur-Martineau, and Christopher Pal. Masked Conditional Video Diffusion for Prediction, Generation, and Interpolation. arXiv, May 2022. arXiv:2205.09853 [cs] type: article.
- [40] Phillip Isola, Jun Yan Zhu, Tinghui Zhou, and Alexei A Efros. Image-to-image translation with conditional adversarial networks. In *CVPR*, 2017.
- [41] Han Zhang, Ian Goodfellow, Dimitris Metaxas, and Augustus Odena. Self-Attention Generative Adversarial Networks. In *ICML*, 2019.
- [42] Alexey Dosovitskiy, Lucas Beyer, Alexander Kolesnikov, Dirk Weissenborn, Xiaohua Zhai, Thomas Unterthiner, Mostafa Dehghani, Matthias Minderer, Georg Heigold, Sylvain Gelly, Jakob Uszkoreit, and Neil Houlsby. An image is worth 16x16 words: Transformers for image recognition at scale. In *ICLR*, 2021.
- [43] Xiaohua Zhai, Alexander Kolesnikov, Neil Houlsby, and Lucas Beyer. Scaling Vision Transformers. pages 12104–12113, 2022.
- [44] Qiangeng Xu, Hanwang Zhang, Weiyue Wang, Peter Belhumeur, and Ulrich Neumann. Stochastic Dynamics for Video Infilling. pages 2714–2723, 2020.
- [45] C. Schuldt, I. Laptev, and B. Caputo. Recognizing human actions: a local SVM approach. In *ICPR*, 2004.
- [46] Frederik Ebert, Chelsea Finn, Alex X. Lee, and Sergey Levine. Self-supervised visual planning with temporal skip connections. In *CoRL*, 2017.
- [47] Thomas Unterthiner, Sjoerd van Steenkiste, Karol Kurach, Raphaël Marinier, Marcin Michalski, and Sylvain Gelly. FVD: A new Metric for Video Generation. In *ICLR Workshop*, 2019.
- [48] Richard Zhang, Phillip Isola, Alexei A Efros, Eli Shechtman, and Oliver Wang. The unreasonable effectiveness of deep features as a perceptual metric. In *CVPR*, pages 586–595, 2018.
- [49] Yunbo Wang, Zhifeng Gao, Mingsheng Long, Jianmin Wang, and Philip S. Yu. PredRNN++: Towards A Resolution of the Deep-in-Time Dilemma in Spatiotemporal Predictive Learning. In *ICML*, 2018.
- [50] Beibei Jin, Yu Hu, Qiankun Tang, Jingyu Niu, Zhiping Shi, Yinhe Han, and Xiaowei Li. Exploring Spatial-Temporal Multi-Frequency Analysis for High-Fidelity and Temporal-Consistency Video Prediction. In *CVPR*, 2020.
- [51] Yunbo Wang, Lu Jiang, Ming-Hsuan Yang, Li-Jia Li, Mingsheng Long, and Li Fei-Fei. Eidetic 3D LSTM: A Model for Video Prediction and Beyond. In *ICLR*, 2018.
- [52] Jiahao Su, Wonmin Byeon, Jean Kossaifi, Furong Huang, Jan Kautz, and Animashree Anandkumar. Convolutional Tensor-Train LSTM for Spatio-temporal Learning. In *NeurIPS*, 2020.
- [53] L. Castrejon, N. Ballas, and A. Courville. Improved Conditional VRNNs for Video Prediction. In *ICCV*, October 2019.
- [54] Ilya Loshchilov and Frank Hutter. SGDR: Stochastic Gradient Descent with Warm Restarts. In *ICLR*, 2017.

## Supplemental Materials: Continuous conditional video synthesis by neural processes

### A. Table of important acronyms and notations

NPVS:	Neural process for conditional video synthesis
VFI:	Video frame interpolation
VFP:	Video future frame prediction
VPE:	Video past frame extrapolation
VRC:	Video random missing frames completion
NPs:	Neural processes
INRs:	Implicit neural representations
FFN:	Fourier feature network
SIREN:	Sinusoidal representation networks
MLP:	Multiple layer perceptron
CNN:	Convolutional neural network
ConvLSTMs:	Convolutional-LSTMs
$V_C$ :	Context video frames
$V_T$ :	Target video frames
$X_C$ :	Context coordinate representations
$Y_C$ :	Context video frame features
$X_T$ :	Target coordinate representations
$Y_T$ :	Target video frame features
$M_C$ :	Output feature of $\mathcal{T}_E$ given $X_C$ and $Y_C$
$M_T$ :	Output feature of $\mathcal{T}_E$ given $X_T$ and $Y_T$
$z_e$ :	event variable
$\mathcal{T}_E$ :	Transformer encoder
$\mathcal{T}_D$ :	Transformer decoder
$E_C$ :	Context event CNN encoder
$E_T$ :	Target event CNN encoder

Table S1. Table of important acronyms and notations

## B. Implementation details

### B.1 Training details

**Training of the autoencoder.** For all datasets, the dimension of visual features is set to be  $H = 8, W = 8, D = 512$ . An Adam optimizer with a learning rate of  $1e^{-4}$  is used for the training. **Training of the NPs-based predictor.** For all datasets,  $\gamma = 0.01$ . For BAIR and SM-MNIST,  $\beta = 1e^{-6}$ . For KTH,  $\beta = 1e^{-8}$ . The predictors are trained by AdamW, we take a cosine annealing learning rate scheduler with warm restarts [54] at every 150 epochs, the maximum learning rate is  $1e^{-4}$  and the minimum learning rate is  $1e^{-7}$ . Gradient clipping is applied to  $\mathcal{T}_E$  and  $\mathcal{T}_D$  during training. Please visit <https://github.com/NPVS/NPVS> for the code.

### B.2 Architecture of VidHRFormer block

For the convenience of the readers, we have redrawn the architecture of VidHRFormer block [38] in Figure S1.

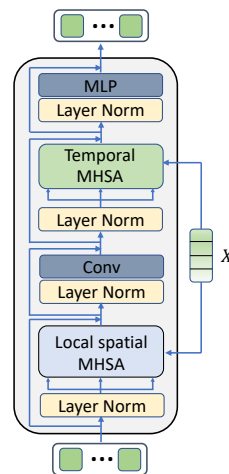


Figure S1. Architecture of VidHRFormer [38].

### B.3 Architecture of Event encoder $E_C$ and $E_T$

Both  $E_C$  and  $E_T$  are implemented by a small neural network with three  $Conv - BN - ReLU$  layers and two  $Conv$  heads to output  $\mu$  and  $\sigma$  respectively. In the case of the deterministic model,  $E_C$  only includes one  $Conv$  head to output  $z_e$ . The architecture of  $E_C$  and  $E_T$  are shown in Figure S2.

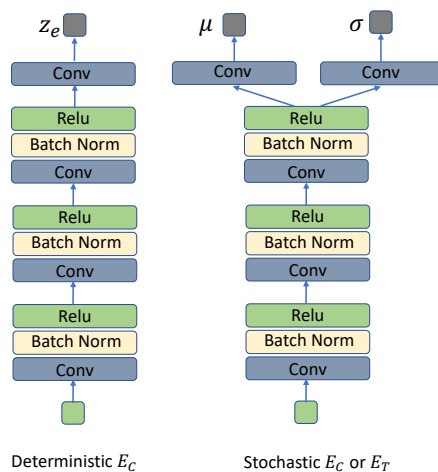


Figure S2. Architecture of the Event encoders.

## C. Datasets introduction

**KTH.** KTH [45] dataset includes grayscale videos of 6 different human actions. Following the experimental setup of

previous work, we take persons 1-16 as training set, and persons 17-25 as test set. Random horizontal flips and vertical flips are applied to each video clip as data augmentation.

For video prediction tasks, the challenges of KTH dataset are introduced by the entry and exit of humans from the scene for some actions, like walking and running, and also the large movements of some actions.

**BAIR.** BAIR [46] dataset includes RGB video clips of a robot arm randomly moving over a table with small objects. The training and test sets are defined by the creators of BAIR. There is no data augmentation for BAIR during training.

The challenge of BAIR is introduced by the fully random movements of the robot arm, thus video prediction models need to take into account the stochasticity for a good prediction.

**SM-MNIST.** Stochastic Moving MNIST (SM-MNIST) [5] is a synthetic dataset includes videos of two randomly moving MNIST characters within a square region. There is no data augmentation for SM-MNIST during training.

Similar to BAIR dataset, one challenge for SM-MNIST dataset is the stochasticity. Another challenge comes from the overlapping of two characters, specifically, the motion before or after the overlapping is difficult to predict.

## D. Qualitative examples

### D.1 Unified model

Here we show another example (see Figure S3) of the unified model for all four different conditional video synthesis tasks. For video examples of different tasks with different frame rates, please visit <https://github.com/NPVS/NPVS>.

### D.2 Task-specific VFI

We present uncurated VFI examples of all three datasets by task-specific *NPVS-D* models, see Figure S4, Figure S5 and Figure S6. Please visit <https://github.com/NPVS/NPVS> for video examples.

### D.3 Task-specific VFP

We present uncurated VFP examples of all three datasets by task-specific *NPVS-D* models, see Figure S8, Figure S9 and Figure S10. Please visit <https://github.com/NPVS/NPVS> for video examples.

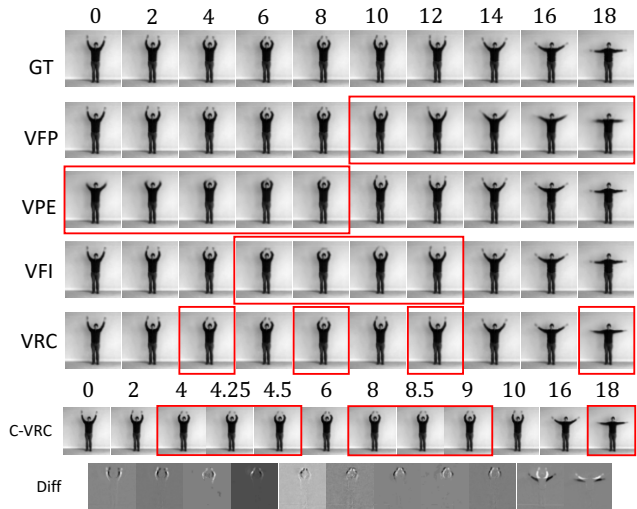


Figure S3. One model for all tasks. Frames inside the red boxes are target frames generated by the model. C-VRC denotes continuous VRC. Diff are the difference images between neighboring frames of C-VRC to show that they are all different and that the temporal coordinates are taken into account.

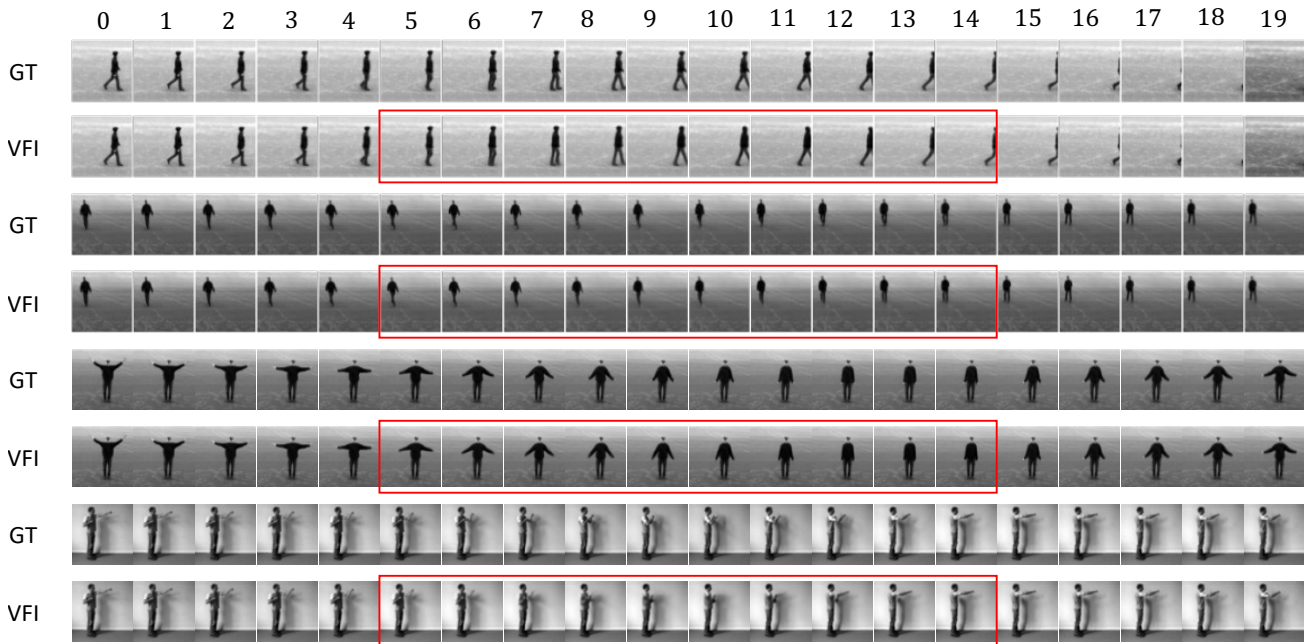


Figure S4. VFI examples on KTH by a Task-specific  $NPVS-D (10 \rightarrow 10)$  model. Frames inside the red boxes are target frames generated by the model.



Figure S5. VFI examples on SM-MNIST by a Task-specific  $NPVS-D (10 \rightarrow 5)$  model. Frames inside the red boxes are target frames generated by the model.

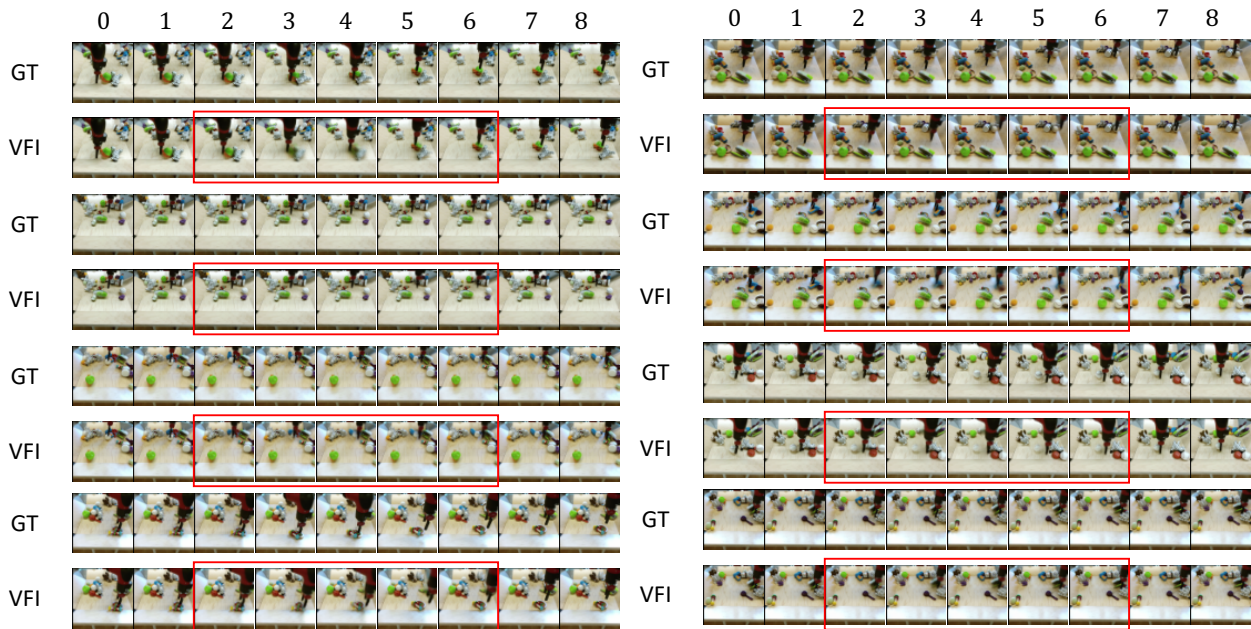


Figure S6. VFI examples on BAIR by a Task-specific *NPVS-D* ( $4 \rightarrow 5$ ) model. Frames inside the red boxes are target frames generated by the model.

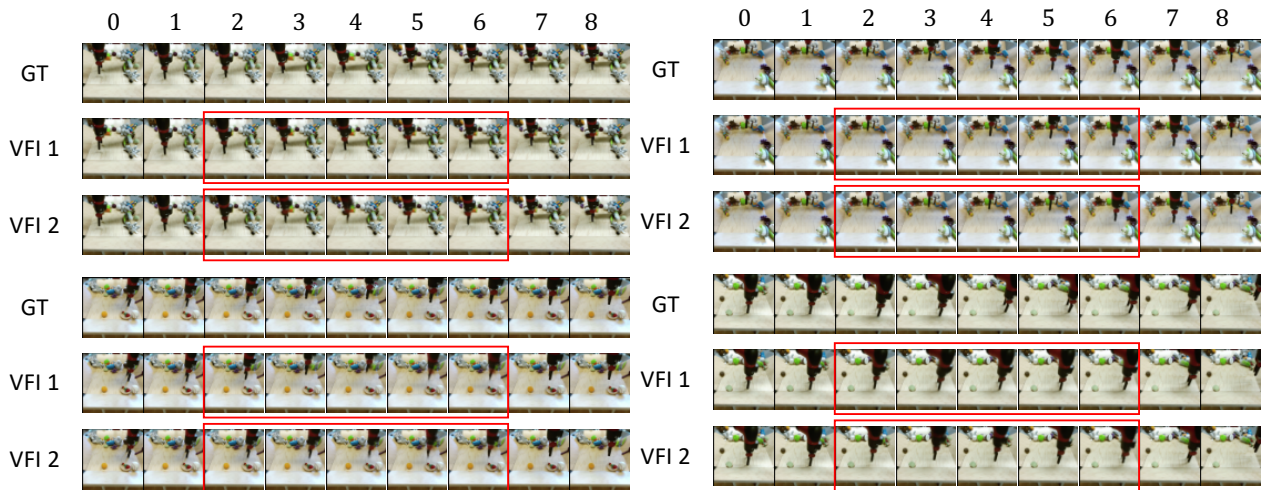


Figure S7. VFI examples on BAIR by a Task-specific *NPVS-S* ( $4 \rightarrow 5$ ) model. Frames inside the red boxes are target frames generated by the model. VFI 1 and VFI 2 denote two different random interpolations given the same contexts.

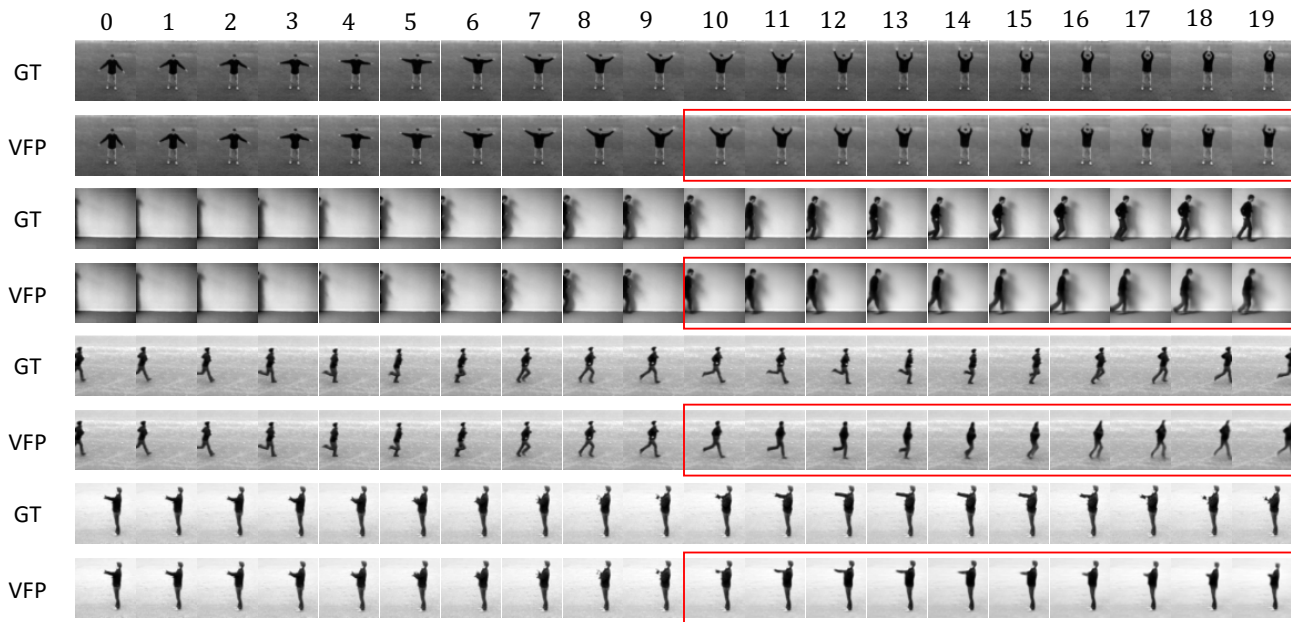


Figure S8. VFP examples on KTH by a Task-specific *NPVS-D* ( $10 \rightarrow 10$ ) model. Frames inside the red boxes are target frames generated by the model.

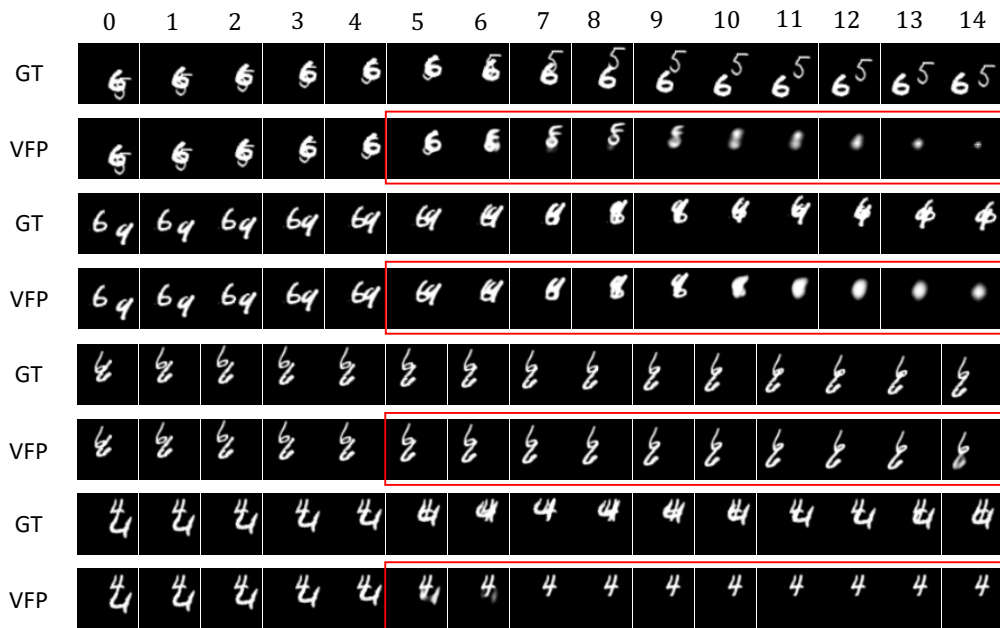


Figure S9. VFP examples on SMMNIST by a Task-specific *NPVS-D* ( $5 \rightarrow 10$ ) model. Frames inside the red boxes are target frames generated by the model.

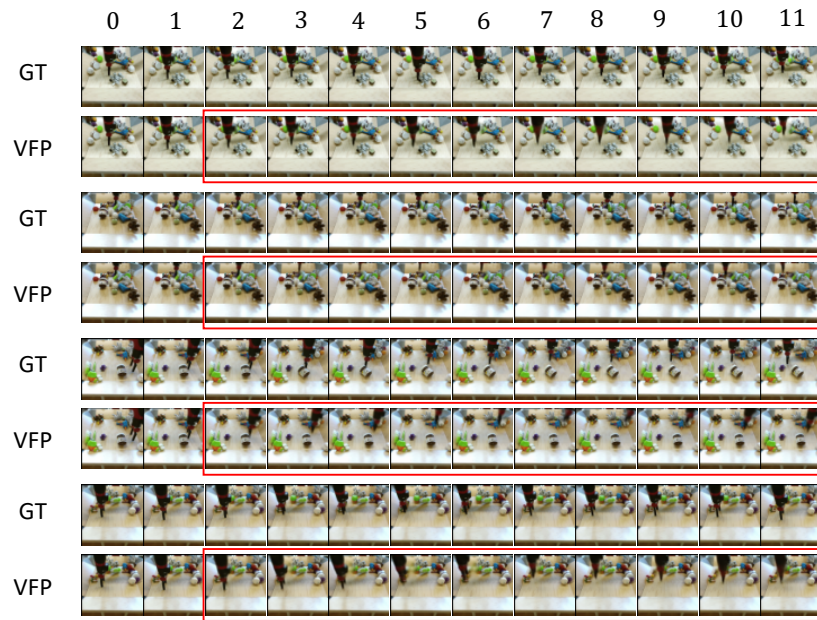


Figure S10. VFP examples on BAIR by a Task-specific *NPVS-D* ( $2 \rightarrow 10$ ) model. Frames inside the red boxes are target frames generated by the model.

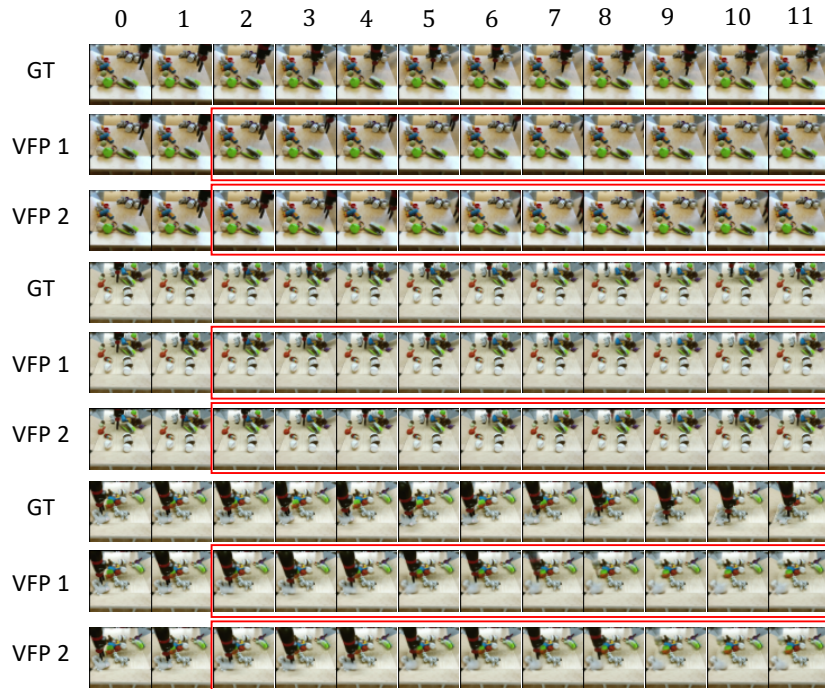


Figure S11. VFP examples on BAIR by a Task-specific *NPVS-S* ( $2 \rightarrow 10$ ) model. Frames inside the red boxes are target frames generated by the model. VFP 1 and VFP 2 denote two different random interpolations given the same contexts.